JCB Journal of Cell Biology

ARTICLE

Rsp5 Ubiquitin ligase–mediated quality control system clears membrane proteins mistargeted to the vacuole membrane

Richa Sardana, Lu Zhu, and Scott D. Emr

Maintenance of organelle identity is profoundly dependent on the coordination between correct targeting of proteins and removal of mistargeted and damaged proteins. This task is mediated by organelle-specific protein quality control (QC) systems. In yeast, the endocytosis and QC of most plasma membrane (PM) proteins requires the Rsp5 ubiquitin ligase and ART adaptor network. We show that intracellular adaptors of Rsp5, Ear1, and Ssh4 mediate recognition and vacuolar degradation of PM proteins that escape or bypass PM QC systems. This second tier of surveillance helps to maintain cell integrity upon heat stress and protects from proteotoxicity. To understand the mechanism of the recognition of aberrant PM cargos by Ssh4–Rsp5, we mistarget multiple PM proteins de novo to the vacuolar membrane. We found that Ssh4–Rsp5 can target and ubiquitinate multiple lysines within a restricted distance from the membrane, providing a fail-safe mechanism for a diverse cargo repertoire. The mistargeting or misfolding of PM proteins likely exposes these lysines or shifts them into the "ubiquitination zone" accessible to the Ssh4–Rsp5 complex.

Introduction

Protein quality control (QC) and surveillance pathways perform the critical task of selectively recognizing and degrading aberrant proteins. Localized, organelle-specific QC systems sample a wide array of targets and need to discriminate between "normal" and "abnormal" proteins while also accounting for spatial and temporal considerations. This task necessitates multiple mechanisms to effectively recognize protein damage, mislocalization, and otherwise normal proteins whose function is no longer required (MacGurn et al., 2012). Accumulation of mislocalized or damaged membrane proteins can be particularly detrimental by interfering with essential membrane processes such as signal transduction or membrane permeability. A protein that is stable at the plasma membrane (PM) also traffics through several other organelles in the secretory and endocytic pathways in its lifetime. Therefore, a combination of sequential QC systems can monitor these membrane proteins as they pass from one compartment to another. For instance, the ER-associated degradation (ERAD) machinery identifies folding-deficient membrane and secretory proteins in the ER and targets them for proteosomal degradation in the cytoplasm (Berner et al., 2018). On the other hand, most post-ER QC mechanisms for membrane proteins target them for degradation via trafficking to the lysosome (MacGurn et al., 2012). The cytosolic domains of membrane proteins are accessible to the compartment specific Ubiquitin (Ub)–protein ligase complexes and serve as sites of Ub modification to mark them for degradation.

Rsp5, the yeast homologue of human Nedd4 HECT E3 Ub ligases, plays a major role in Ub-dependent trafficking in the endocytic system. Ub serves as the signal for recognition by endocytic machinery, and for sorting at the multivesicular body (MVB) endosomes and at the vacuole membrane (VM). Rsp5 is a cytosolic protein and is recruited to target proteins in distinct organelles by specific "adaptors" that facilitate its broad substrate range and accessibility. The dependence of Rsp5 on the adaptor for target accessibility also provides a built-in mechanism to restrict and regulate Rsp5 function or activity. Rsp5 adaptors contain one or more PY motifs (PPxY) that mediate their interaction with the three WW domains in Rsp5 (Rotin et al., 2000). At the PM, Rsp5 function is facilitated by its recruitment via a network of arrestin-related trafficking adaptors (ARTs) that allows endocytic remodeling of PM composition upon changes in nutrient availability and environmental stress (Lin et al., 2008; Zhao et al., 2013). Intracellular cargos are exposed to Rsp5 via adaptors such as Bsd2 and Ear1 to initiate sorting into MVBs (Belgareh-Touzé et al., 2008; Léon and Haguenauer-Tsapis, 2009) and via Ssh4 at the VM (Li et al., 2015b; Zhu et al., 2017). Ubiquitination of the

Department of Molecular Biology and Genetics, Weill Institute for Cell and Molecular Biology, Cornell University, Ithaca, NY.

Correspondence to Scott D. Emr: sde26@cornell.edu.

cargo proteins initiates a cascade of events that drives the specific packaging of the ubiquitinated cargo by endosomal sorting complexes required for transport (ESCRT) complexes into vesicles that bud into the lumen of endosomes or vacuoles (Henne et al., 2013; Piper et al., 2014). While the downstream mechanisms of cargo sorting for degradation have been extensively investigated, our understanding of cargo recognition by various Rsp5 adaptors is still rudimentary. The cargo intrinsic degradation signal readout by the adaptor and Ub-ligase complex is thought to be embedded in the sequence or structure of the membrane protein itself. Additionally, it is unclear if there is crosstalk between the various Rsp5-adaptor networks in the endocytic pathway.

This work highlights how multiple Rsp5-adaptor networks integrate into the larger suite of protein QC mechanisms. We show that sequential surveillance by PM and intracellular Rsp5 adaptors prevents inappropriate accumulation of PM proteins endocytosed via Ub-dependent and independent processes. The tiered endocytic surveillance structure ensures efficient housekeeping and becomes critical for maintenance of cellular fitness in conditions of environmental stress. To investigate how intracellular adaptors recognize endocytosed cargos, we created aberrant variants of PM proteins that traffic directly to the VM via the AP-3 pathway. This served as a useful tool to specifically focus on recognition of mislocalized proteins on the VM, isolating it from the successive ubiquitination steps at the PM and endosome. In contrast to recognition of cargo-specific sequence motifs at the PM by ART–Rsp5 complexes and other endocytic components (Piao et al., 2007; Guiney et al., 2016), we show that the recognition of these cargos at the vacuole by the Ssh4–Rsp5 complex is quite promiscuous, targeting unmasked lysines within a restricted distance from the membrane. This provides a "fail-safe" mechanism to capture a diverse set of cargos that were not detected by or escaped from MVB sorting, preventing the accumulation of aberrant proteins at the VM and preserving the identity of the vacuole, the terminal organelle of the endocytic pathway.

Results

Intracellular Rsp5 adaptors ensure vacuolar targeting of endocytosed PM cargo that escape MVB sorting

Endocytosis of the cell wall integrity sensor Wsc1 has been previously reported to be dependent on the interaction between the NPFxD motif in its cytosolic tail and the SHD1 domain of Sla1 (Piao et al., 2007). WT Wsc1 tagged with GFP exhibits polarized cell surface localization with enrichment at the tips of emerging buds and the bud neck, as well as intracellular signal in the vacuolar lumen indicative of degradation by vacuolar proteases (Fig. 1 A). As expected, Wsc1 NPF>AAA mutant defective for binding to Sla1 was blocked on the PM and lost its polarized distribution (Fig. 1 A; Piao et al., 2007; Wilk et al., 2010). To test whether lysine ubiquitination plays a role in regulating intracellular Wsc1 localization, we mutated all six lysines in the C-terminal cytosolic tail of Wsc1 ($Wsc1^{6K>R}$). The $Wsc1^{6K>R}$ mutant could be endocytosed but accumulated on the limiting membrane of the vacuole (Figs. 1 A and S1 A). Both WT Wsc1 and the 6K>R mutant were stabilized at the PM in the endocytosis-defective mutant *end3*Δ, confirming that $Wsc1^{6K>R}$ accumulates at the VM following endocytosis rather than by altered biosynthetic trafficking (Fig. S1 B). End3 is required for early steps of endocytic vesicle formation, and its absence strongly blocks both Ub- and NPFxD-mediated endocytosis (Bénédetti et al., 1994; Tan et al., 1996). Thus, although endocytosis of Wsc1 is Ub independent, its intracellular sorting to the vacuole lumen for degradation appears to depend on the ubiquitination of its cytosolic tail.

The ubiquitination of most cargos throughout the endocytic system requires the recruitment of Rsp5 Ub ligase to the cargo by PY motif–containing adaptor proteins (Belgareh-Touzé et al., 2008). Early characterization of Ear1 and Ssh4 identified them as a homologous pair of Rsp5 adaptors required for MVB sorting at the endosomes (Léon et al., 2008). Subsequent studies elucidated distinct localization and functional sites for Ear1 and Ssh4 at the endosome and VM, respectively (Léon et al., 2008; Li et al., 2015b; Zhu et al., 2017). We asked if Ear1 and/or Ssh4 were required for the sorting of Wsc1 to the vacuolar lumen. Endocytosed Wsc1-GFP indeed accumulated on the VM in an *ssh4*Δ *ear1*Δ double mutant, similar to the $Wsc1^{6K>R}$ mutant, indicating that Ear1 and Ssh4 can recognize Wsc1 for intracellular ubiquitination (Fig. 1 B). Cysteine to alanine substitution mutants in the extracellular cysteine-rich domain of Wsc1 have previously been reported to be defective for clustering at the cell surface, and the mutant protein is rapidly endocytosed, resulting in accumulation in the vacuole lumen (Heinisch et al., 2010; Kock et al., 2016). A GFP-tagged $Wsc1^{C69,71A}$ mutant also strongly accumulated on the VM in the *ssh4*Δ *ear1*Δ double mutant (Fig. 1 C). However, Wsc1-GFP sorting was unaffected in *ssh4*Δ or *ear1*Δ single mutants, suggesting that cargos encounter Ear1 and Ssh4 at successive steps along the endocytic route (Fig. S1 C). As expected, the dependence on Ear1 and Ssh4 was less evident for GFP-tagged Lyp1 and Mup1 that are ubiquitinated at the cell surface before endocytosis (Figs. 1 D and S1 D). To address whether these cargos accumulate at the VM in the *ssh4*Δ *ear1*Δ mutant, we conjugated Lyp1 and Mup1 to a pH-sensitive GFP variant, pHluorin, whose fluorescence is quenched in the acidic pH of the vacuolar lumen. Indeed, distinct VM accumulation could be observed for Lyp1-pHluorin at steady state (Fig. 1 D) as well as upon stimulation of Mup1 endocytosis by addition of methionine (Fig. S1 D). The reduction in sorting to the vacuole lumen in *ssh4*Δ *ear1*Δ mutant versus WT cells was quantified by immunoblotting (Lyp1 ∼32%, Mup1 ∼18%, and Wsc1 ∼71%) as well as by fluorescence microscopy (Lyp1 ∼29%; Fig. S1, E and F). Likewise, Ssh4 function was required for the clearance of v-SNARE Snc1 from the VM in a sorting nexin *snx4*Δ mutant that is defective in recycling Snc1 from the endosome (Fig. 1 E; Hettema et al., 2003). Failure to recycle Snc1 from the endosome results in its delivery to and accumulation on the VM upon endosome–vacuole fusion.

Based on these observations, we conclude that intracellular adaptors of Rsp5 play a key role in regulating the fate of endocytosed cargos. Furthermore, since the vacuole is the terminal destination for endocytic cargos, Ssh4 also provides the critical final checkpoint for removal of non-VM proteins that escape MVB sorting due to postendocytic deubiquitination or defects in recycling. The distinct cellular localization of Rsp5 adaptors in sequential compartments of the endocytic system provides a mechanism to prevent accumulation of aberrant membrane cargos and maintain organelle identity.

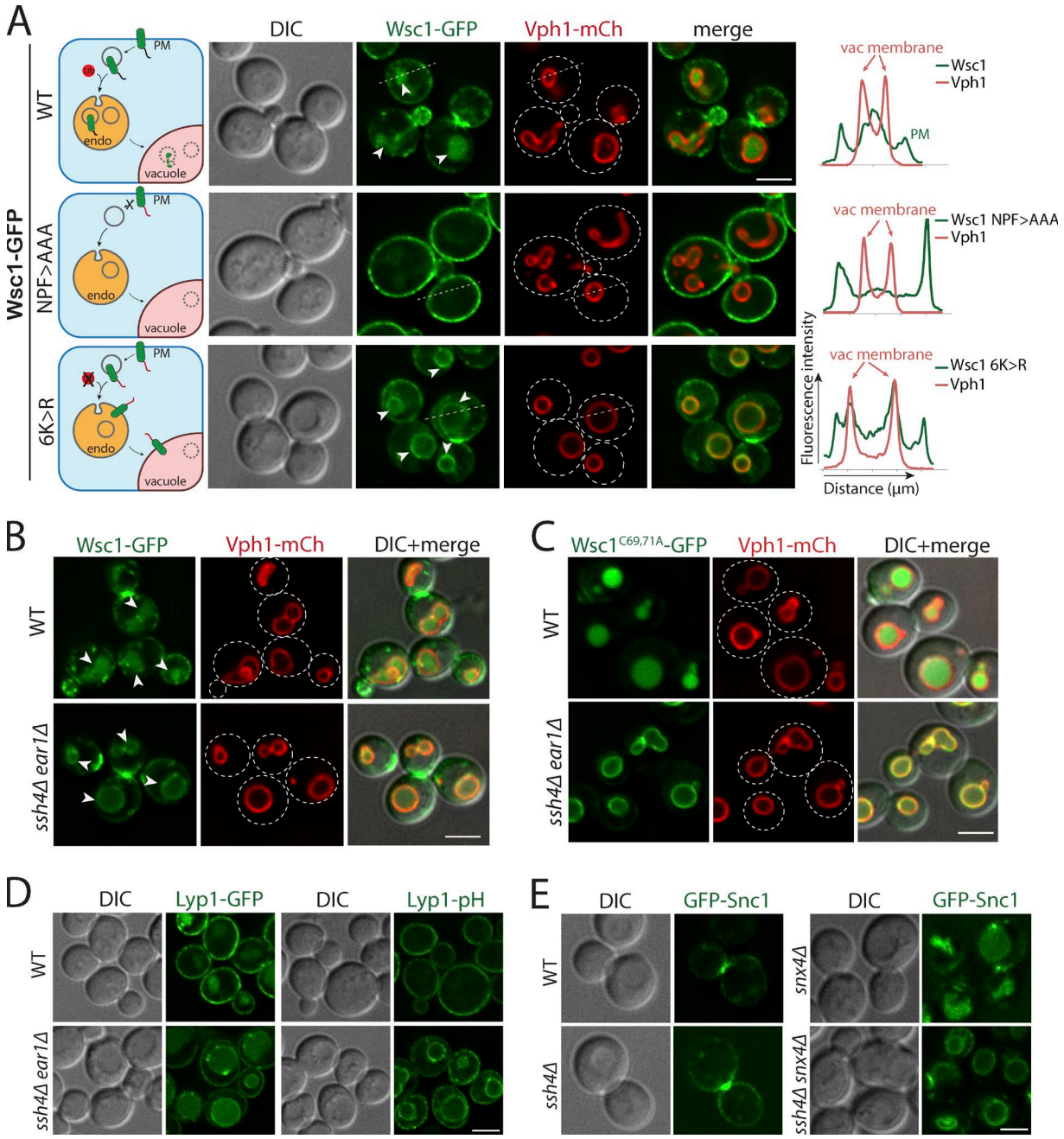

Figure 1. **Intracellular Rsp5 adaptors are required for vacuolar sorting of multiple endocytosed PM cargos. (A)** Live-cell fluorescence and differential interference contrast (DIC) imaging of a GFP-tagged cell wall integrity sensor, Wsc1, and mutants lacking the Sla1 recognition motif (NPF>AAA) or all cytosolic lysines (6K>R) in WT yeast cells also expressing an mCherry-tagged VM marker, Vph1, a subunit of the vacuolar ATPase V0 domain. The arrowheads point to the vacuolar lumen signal for WT Wsc1 and the VM signal for $Wsc1^{6K>R}$ mutant, respectively. The dashed line indicated on a representative cell for each condition was used to build a line-scan fluorescence profile using ImageJ. Schematic describing the localization phenotype for each condition is illustrated on the left. **(B)** WT and *ssh4Δ ear1Δ* mutant cells expressing Wsc1-GFP. The arrowheads point to the vacuolar lumen signal in WT cells and the VM signal in *ssh4Δ ear1Δ* mutant, respectively. **(C)** WT or *ssh4Δ ear1Δ* mutant yeast cells expressing clustering defective, constitutively endocytosed $Wsc1^{C69,71A}$-GFP. **(D)** WT or *ssh4Δ ear1Δ* double-mutant yeast cells expressing Lyp1 fused to GFP (Lyp1-GFP) or a pH-sensitive pHluorin (Lyp1-pHluorin). **(E)** Fluorescence microscopy of GFP-tagged v-SNARE Snc1 in WT, *ssh4Δ*, *snx4Δ* single mutants and *ssh4Δ snx4Δ* double mutant. Scale bars: 2.5 μm.

PM proteins misdirected to the VM are constitutively degraded by the Ssh4–Rsp5 Ub ligase complex

To understand the molecular basis of intracellular recognition of PM proteins, we needed to distinguish between Ub-ligase recognition events at the VM from that at the PM or endosome. To do so, we devised a strategy to biosynthetically reroute a PM protein directly to the VM. We fused an acidic dileucine (ExxxLL) motif (henceforth referred to as acLL) recognized by the AP-3 adaptor complex at the Golgi to biosynthetically reroute PM-bound proteins directly to the VM (Fig. 2 A; Cowles et al., 1997; Vowels and Payne, 1998). We designed acLL fusions to PM cargos with multiple transmembrane domains (TMDs; Mup1 and Lyp1) as well as a

single TMD (Wsc1; Fig. S2 A). To assess the effect of the addition of the acLL motif, we compared yeast cells expressing GFP-tagged PM or PM-acLL fusion cargos. GFP-tagged Mup1, Lyp1, and Wsc1 exhibited the expected cell surface localization. The addition of acLL motif (Mup1-acLL-GFP, acLL-Lyp1-GFP, and Wsc1-acLL-GFP) efficiently redirected each of these PM proteins away from the PM to the vacuole (Fig. 2 B). Strikingly, all the tested PM-acLL reporters accumulated in the vacuole lumen instead of at the VM at steady state.

To confirm that the localization of PM-acLL cargos was dependent on the recognition of acLL motif by the AP-3 adaptor complex, we expressed Mup1-acLL-GFP in cells lacking Apm3, the μ-subunit of the AP-3 adaptor complex (Cowles et al., 1997). Loss of Amp3 or mutations in the acLL motif (**E**QSP**LL**>>**K**QSP**SQ**) restored the localization of Mup1-acLL-GFP to the PM (Fig. 2, C and D). Finally, while Wsc1-GFP and Mup1-GFP were blocked on the PM, the localization of the PM-acLL variants to the vacuole lumen was unchanged in the endocytosis-defective *end3*Δ mutant (Figs. 2 E and S2 B), indicating that the PM-acLL cargos do not reach the vacuole via a PM or constitutive endocytosis route. Collectively, these data show that PM proteins can be effectively mistargeted to the vacuole by the addition of an accessible acidic dileucine motif recognized by the AP-3 adaptor complex at the Golgi.

AP-3 cargo proteins usually localize to the VM, but the steady-state localization of the PM–acLL reporters was primarily in the vacuole lumen. We hypothesized that the PM-acLL reporters delivered to the VM via AP-3 adaptor–coated vesicles were specifically recognized as aberrant or foreign proteins by the Ssh4–Rsp5 complex and sorted for degradation in the vacuolar lumen. Indeed, all the PM-acLL reporters (Mup1-acLL, Wsc1-acLL, and acLL-Lyp1) were stabilized on the VM in the *ssh4*Δ mutant (Fig. 3 A). The sorting to the vacuolar lumen was also dependent on Rsp5 E3 ligase activity; PM–acLL reporters were blocked on the vacuolar limiting membrane in the hypomorphic mutant, *rsp5*^{G747E} (Fig. 3 B; Fisk and Yaffe, 1999). Because GFP is more resistant to vacuolar hydrolases, vacuolar degradation of the reporters could also be assayed by Western blotting by observing the accumulation of free GFP. Full-length Mup1-acLL-GFP and Wsc1-acLL-GFP were barely detectable in extracts prepared from WT yeast and exhibited a strong accumulation of free GFP. This was completely reversed in the *pep4*Δ mutant, confirming that the degradation was dependent on hydrolases in the vacuolar lumen (Fig. 3, C, D, and F). The degradation was also strongly blocked in *vps4*Δ (ESCRT defective) and *ssh4*Δ mutants corresponding to the lack of sorting to the vacuolar lumen (Fig. 3, E and F; and Fig. S3 A). ESCRT function is required for the efficient delivery of Ssh4 to the VM as well as for the sorting of the ubiquitinated cargos at the VM, manifesting as a block in cargo degradation (Zhu et al., 2017). However, the Tul1 Dsc E3 ligase complex, which has previously been reported to recognize multiple VM cargos for degradation, had no effect (Fig. 3, E and F; Li et al., 2015a). Taken together, these data suggest that the Ssh4–Rsp5 Ub-ligase complex recognizes PM proteins that aberrantly reach the VM and ensure their degradation to prevent accumulation at the VM.

Cytosolic tail of mistargeted cargos is necessary and sufficient for recognition by Ssh4–Rsp5

To decipher the molecular features of aberrant PM proteins that allow their recognition by Ssh4–Rsp5 at the VM, we decided to focus on Wsc1. Wsc1 contains a long extracellular N-terminal tail (264 aa), a single TMD, and a relatively short cytosolic C-terminal tail (93 aa), making it suitable for mutational analysis. The bulky extracellular domain of Wsc1 faces the vacuolar lumen and is trimmed by lumenal proteases in mutants that block Wsc1-GFP or Wsc1-acLL-GFP on the VM. To ascertain if the extracellular domain is required for recognition of Wsc1-acLL-GFP, we deleted the entire extracellular region except the first 25-aa signal peptide (Fig. 4 A). The Wsc1$^{\Delta N}$-acLL-GFP mutant trafficked normally to the vacuole and was efficiently sorted to the lumen for degradation, indicating that this region does not affect recognition of Wsc1 by Ssh4–Rsp5 Ub-ligase complex.

The cytosolic tail of Wsc1 does not contain any known protein domain or motif and is predicted to be flexible. To test the contribution of the cytosolic C-terminal tail and the TMD, we fused them to Atg27, a protein that is stable at the endosome and the VM (Segarra et al., 2015; Suzuki and Emr, 2018; Fig. 4 B). The fusion of the cytosolic domain of Wsc1 was sufficient to sort the Atg27–Wsc1 chimera constitutively into the vacuole lumen in an Ssh4-dependent manner (Fig. 4, B and C). In agreement, the fusion protein was significantly processed to free GFP in WT cells in the Western blotting–based degradation assay, but the processing was completely blocked in the *ssh4*Δ mutant (Fig. 4 D). However, the chimera containing Wsc1 TMD but lacking the C-terminal cytosolic tail was blocked on the VM (Fig. 4, B and C).

To determine which part of the cytosolic tail contributed to this recognition, we constructed a series of C-terminal truncation mutants of the Wsc1-acLL-GFP reporter (Fig. 4 E). The truncation mutants labeled as Wsc1$^{286–378}$, Wsc1$^{286–358}$, Wsc1$^{286–338}$, Wsc1$^{286–318}$, and Wsc1$^{286–298}$ contain the full length (93 aa), 73, 53, 33, or 13 aa of the cytosolic tail of Wsc1, respectively, followed by the acLL motif and GFP to monitor their localization. Curiously, all the C-terminal truncation mutants except Wsc1$^{286–298}$ were quite efficiently sorted into the vacuolar lumen in an Ssh4-dependent manner (Fig. 4 E). This indicated that the features sufficient to ensure Ssh4–Rsp5–mediated degradation of the Wsc1-acLL-GFP cargo were contained within the last 20 aa in the Wsc1$^{286–318}$ mutant. Based on these findings, we concluded that the Ssh4–Rsp5 complex recognizes a feature in the cytosolic tail of cargos to mark them for degradation.

Accessible lysines and their distance from the membrane drive cargo ubiquitination by Ssh4–Rsp5

Intrigued by how the 20-aa stretch on the C-terminal tail of Wsc1 contributed to its degradation and to understand the general principles of Ssh4–Rsp5–mediated recognition, we inspected this sequence more closely (Fig. 5 A). The most striking aspect of this sequence was the presence of three of the six cytosolic lysines of Wsc1. Our simplest hypothesis was that the Wsc1$^{286–298}$ mutant was blocked for degradation because of deletion of the key lysine residue. To determine which lysine was the key substrate for Ub modification by Rsp5, we mutated individual lysines. However,

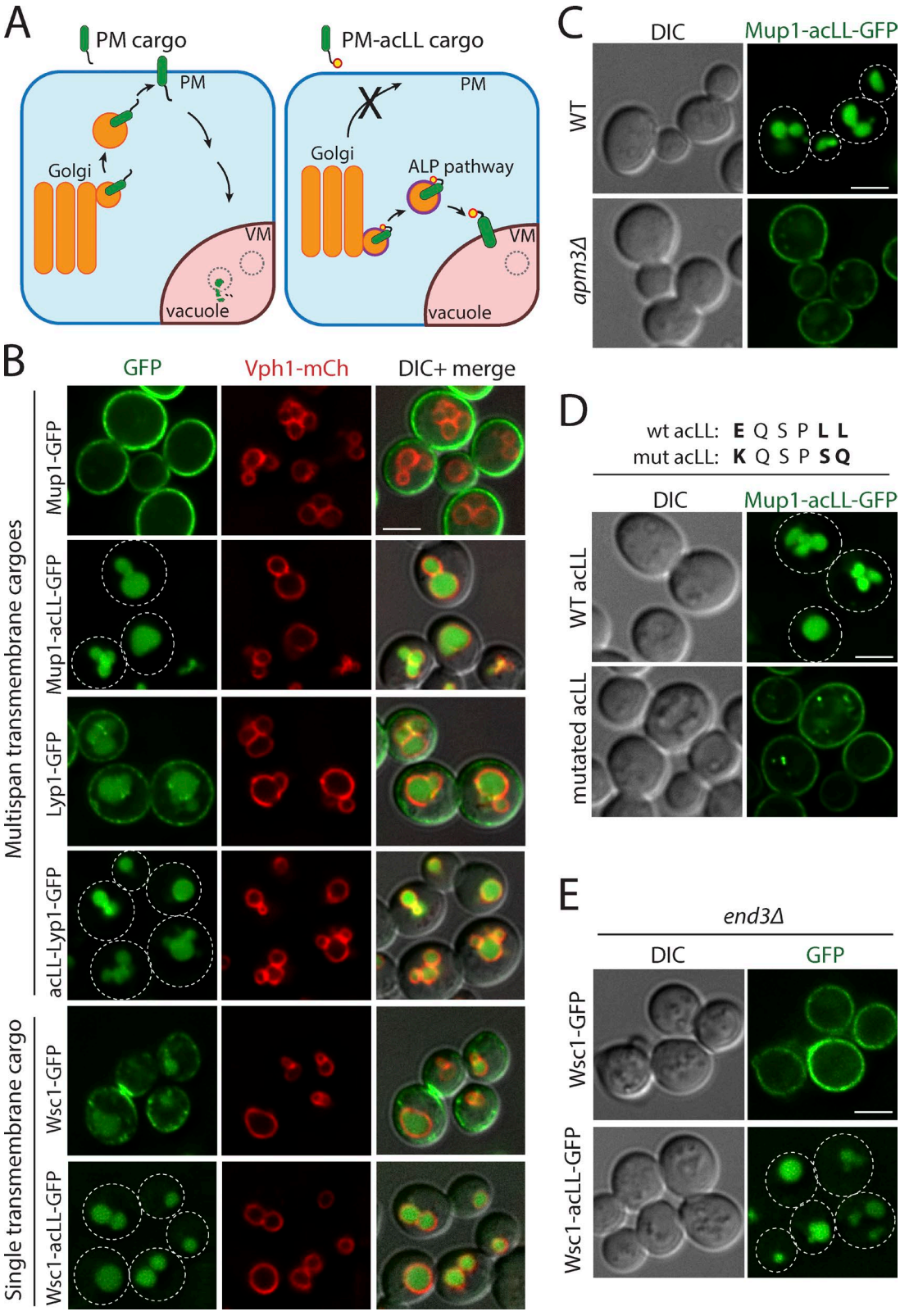

Figure 2. **Addition of acLL motif constitutively mistargets PM proteins to the vacuole. (A)** The strategy for mistargeting PM cargos to the vacuole. PM cargos are normally packaged into secretory vesicles at the Golgi that fuse with the PM (left). Addition of a 6-aa acidic dileucine (**E**QSP**LL**) or acLL motif (indicated by a yellow dot with a red border) to the cytosolic tails of PM proteins (PM-acLL cargo), engages the AP-3 adaptor complex at the Golgi, changes their itinerary and misdirects them to the vacuole via the ALP pathway (right). **(B)** Fluorescence microscopy of WT yeast cells expressing GFP-tagged Mup1, Lyp1, and Wsc1 proteins or acLL-tagged variants (Mup1-acLL, acLL-Lyp1, and Wsc1-acLL). VM marker, Vph1-mCherry. **(C)** WT or *apm3*Δ mutant yeast expressing Mup1-acLL-GFP. **(D)** WT yeast expressing WT or mutated acLL motif fused to Mup1-GFP. **(E)** *end3*Δ mutant yeast expressing GFP tagged Wsc1 or Wsc1-acLL. Scale bars: 2.5 µm.

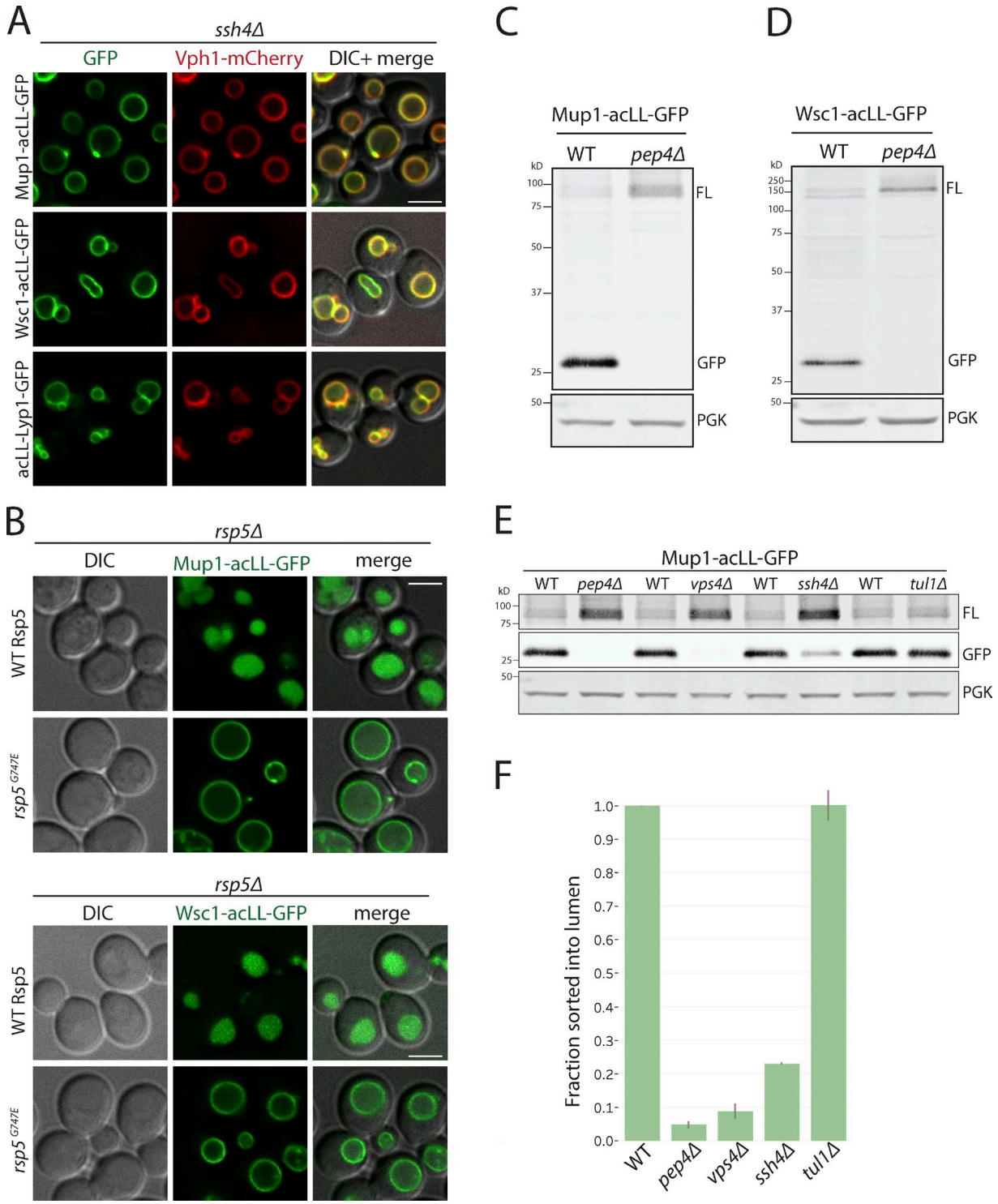

Figure 3. **Vacuolar sorting of mistargeted cargos at the VM requires Rsp5, Ssh4, and ESCRT function. (A)** Fluorescence microscopy of *ssh4Δ* mutant cells expressing Mup1-acLL-GFP, Wsc1-acLL-GFP, and acLL-Lyp1-GFP. Scale bar: 2.5 µm. VM marker, Vph1-mCherry. **(B)** *rsp5Δ* mutant containing plasmid based WT Rsp5 or the hypomorphic allele $rsp5^{G747E}$ also expressing Mup1-acLL-GFP (top) or Wsc1-acLL-GFP (bottom). **(C and D)** Immunoblot analysis on extracts prepared from WT or *pep4Δ* mutant cells expressing Mup1-acLL-GFP (C) or Wsc1-acLL-GFP (D). FL refers to GFP-tagged full-length cargo. Free GFP is more resistant to vacuolar proteases and serves as a proxy for the cargo sorted inside the vacuole lumen. PGK serves as the loading control. **(E)** Immunoblot analysis comparing WT, *pep4Δ*, *vps4Δ*, *ssh4Δ* and *tul1Δ* mutant cells expressing Mup1-acLL-GFP reporter as described in C. Lanes 1 and 2 are the same as shown in C. **(F)** Quantitation of three replicates of immunoblots described in E. The fraction of Mup1-acLL-GFP sorted into the lumen refers to the ratio of the processed GFP to the total reporter levels. Error bars indicate standard error of the measurements.

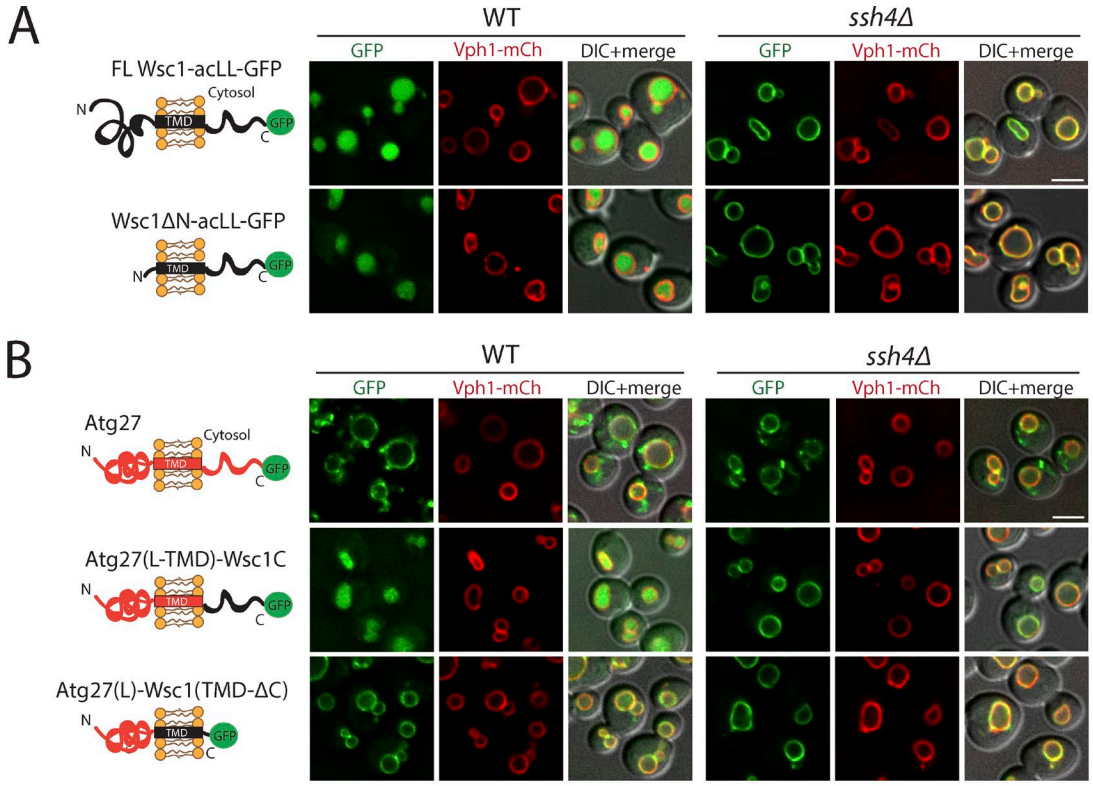

C

Domain: Lumenal	TMD	Cytosolic	Localization
Atg27	Atg27	Atg27	VM
Atg27	Atg27	Wsc1	Lumen
Atg27	Wsc1	Wsc1	Lumen
Atg27	Wsc1	-	VM

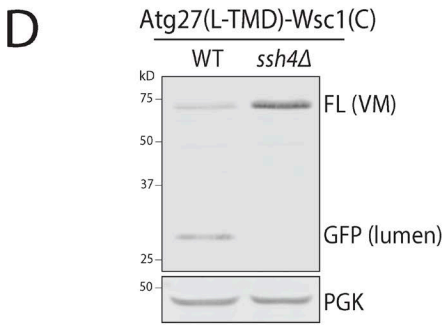

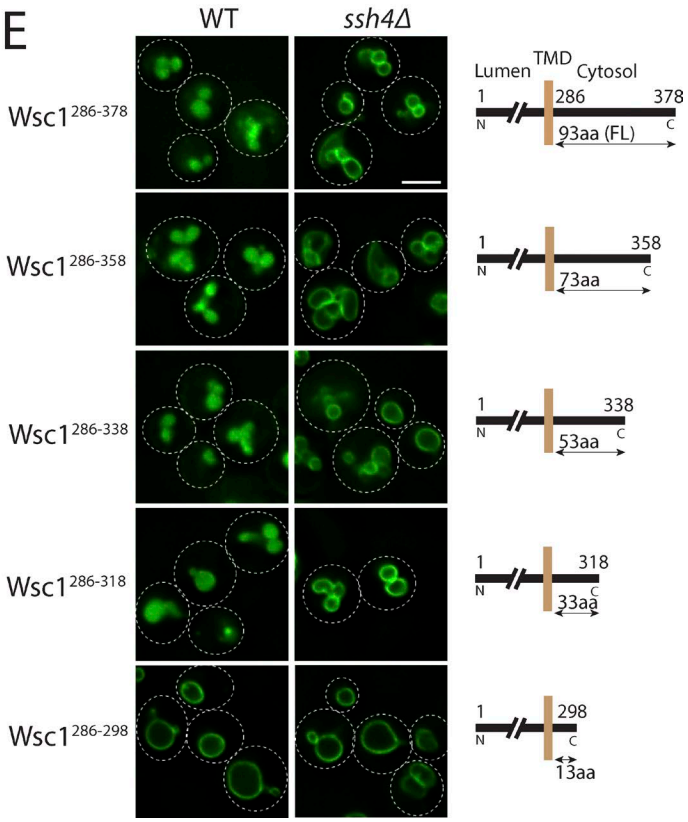

Figure 4. **The Ssh4–Rsp5 complex recognizes a feature in the cytosolic tails of cargos. (A)** Fluorescence microscopy of WT and *ssh4*Δ cells expressing full-length Wsc1-acLL-GFP or Wsc1$^{\Delta N}$ mutant lacking the entire lumenal domain (except the signal peptide). Scale bar: 2.5 µm. VM marker, Vph1-mCherry. **(B)** WT and *ssh4*Δ cells expressing chimeric proteins containing fusion of just the cytosolic tail or just the TMD of Wsc1 and acLL-GFP to the lumenal domain of a stable VM protein, Atg27. The cartoons on the left indicate the topology of each chimera. **(C)** Table summarizing the results of the fluorescence microscopy analysis described in B. **(D)** Immunoblot analysis of WT and *ssh4Δ* extracts expressing the Atg27$^{(L\text{-}TMD)}$-Wsc1$^{(C)}$-acLL-GFP chimera. **(E)** WT and *ssh4*Δ mutant cells expressing C-terminal truncations of the cytosolic tail of Wsc1 as indicated by the schematics on the right, fused to acLL and GFP. Dashed lines indicate the cell periphery.

none of the lysines in the 20-aa stretch (aa 299–318) when mutated individually had any effect on the sorting and degradation of Wsc1-acLL-GFP by localization or protein degradation assays (Fig. 5, B–D; and data not shown). The degradation of the mutants was also dependent on Ssh4. A global analysis of substrate ubiquitination sites had previously reported a distinct compositional bias for the presence of acidic amino acids next to ubiquitinated lysines as compared with nonubiquitinated sites (Radivojac et al., 2010). Two of the lysines (at positions 301 and 315) in the Wsc1 C-terminal tail are adjacent to acidic amino acids. However, even combining the substitution of the potentially favorable lysines at K301 and K315 with arginine (denoted as 2KR mutant) only resulted in a partial block in lumenal sorting and degradation (Fig. 5, B–D). These observations indicated that multiple lysine residues in the cytosolic tail of Wsc1 can be modified by Rsp5. Accordingly, mutating four lysines (4KR; K301, 315, 338, and 365) or all six lysines (6KR; K293, 301, 308, 315, 338, and 365) exposed to the cytosol completely blocked lumenal sorting as well as degradation of the misdirected cargo (Fig. 5, B–D). To confirm that the block is indeed due to lack of ubiquitination, we coexpressed WT or 6KR Wsc1-acLL-GFP in WT or *ssh4*Δ cells (also lacking Doa4, Pep4, and Prb1 to stabilize ubiquitinated species; Amerik et al., 2000). Immunoprecipitation of Wsc1-acLL-GFP, followed by probing the immunoprecipitates with anti-GFP as well as anti-Ub antibodies, revealed the accumulation of higher-molecular-weight ubiquitinated species of Wsc1-acLL-GFP in WT but lacking in *ssh4*Δ or 6KR mutant (Fig. 5 E).

Since lysines in multiple positions could serve as substrates for Ssh4–Rsp5–mediated ubiquitination, it is interesting to note that the sole available lysine K293 in Wsc1$^{286–298}$ truncation mutant could not facilitate sorting (Fig. 4 E). We reasoned that effective ubiquitination can only occur at lysine residues that are correctly positioned to allow interaction with and selection by Ssh4–Rsp5. Therefore, lysines too close or too far from the membrane may be less likely to serve as good targets. To test this, we introduced peptide linkers of varying lengths between the TMD and the C-terminal tail of Wsc1 (Fig. 6 A). The peptide linkers containing (EAAAR [i, i + 4]) repeats are expected to fold into rigid α-helical conformations (Huyghues-Despointes et al., 1993). In addition, the $(EAAAR)_n$ linkers are devoid of any lysines and hence could not be ubiquitinated themselves. Indeed, while addition of a 25-aa rigid linker, $(EAAAR)_5$, between the TMD and the C-terminal tail allowed efficient sorting and degradation, increasing the linker length to 50 or 70 aa completely blocked sorting into the vacuolar lumen (Fig. 6 A).

To more finely assess the effect of distance of the lysine from the membrane in the context of the unstructured cytosolic tail of Wsc1, we first mutated all six lysines and then introduced a single lysine in increments of 7–10 aa along the cytosolic tail (Fig. 6 B). We found that while a single lysine roughly between 10 and 38 aa from the membrane was able to support sorting into the vacuolar lumen for degradation, a lysine residue anywhere less or greater than that range was blocked on the VM (Fig. 6, B and D; and Fig. S4, A and B). Furthermore, moving the lysine closer to the membrane by deletion of 20 aa upstream of the lysine allowed efficient sorting if the new lysine position moved to between 10 and 38 aa from the membrane (Fig. 6, C and D; and Fig. S4 A).

We next wondered if resident VM proteins could be made substrates of Ssh4–Rsp5 Ub ligase by introduction of an appropriately placed lysine in their cytosolic tails. Indeed, we have previously reported that addition of a 38-aa streptavidin-binding peptide (SBP) between Ypq1 and GFP (Ypq1-SBP-GFP) results in constitutive sorting of Ypq1 into the vacuole lumen (Zhu et al., 2017). Closer inspection of the sequence revealed that the constitutive degradation is due to the presence of a lysine in the SBP tag, positioned 20aa from the VM in the Ypq1-SBP-GFP fusion protein. This sorting is dependent on Ssh4, and mutating the lysine to arginine stabilized the fusion protein on the VM (Fig. 7 A). To specifically test this in the context of the native cytosolic tails of resident VM proteins, we mutated a single-residue ∼18 aa from the membrane to a lysine in the cytosolic tail of Atg27 (L>K) and Ypl162c (N>K). The substitution was strikingly effective in serving as a degron and resulted in constitutive sorting these proteins to the vacuolar lumen (Fig. 7, B and C).

Finally, we predicted that addition of a linker in Ssh4 instead of the cargo should mirror the observed phenotype. We added linkers of varying lengths (15, 30, 45, and 60 aa) between the TMD and cytosolic tail of Ssh4 and tested their ability to sort Wsc1-acLL-GFP and Wsc1^{50aaLinker}-acLL-GFP. Indeed, adding linkers of increasing lengths made Ssh4 progressively worse for sorting of Wsc1-acLL and better for sorting of Wsc1-^{50aaLinker}-acLL-GFP (Fig. 7 D). Taken together, we conclude that rather than recognition of a specific sequence motif, aberrant cargo sorting by Ssh4–Rsp5 at the VM is largely determined by the availability of unmasked lysines in the ubiquitination zone appropriately positioned relative to the membrane (Fig. 7 E).

Surveillance by Rsp5 adaptors along the endocytic pathway protects yeast from proteotoxic stress

Previous work from our laboratory elucidated that the ART–Rsp5 network comprises a key PM QC system to ensure removal of misfolded cell-surface proteins upon thermal stress (Zhao et al., 2013). Heat stress, resulting in protein misfolding, was reported to significantly increase the flux of endocytosis from the cell surface. The inability to down-regulate misfolded cell-surface proteins in *rsp5-ww* mutant or mutants lacking cell-surface adaptors for Rsp5, such as Art1, resulted in temperature sensitivity and loss of cell-surface integrity (Zhao et al., 2013). Our findings suggest that intracellular adaptors of Rsp5 allow the recognition and clearance of endocytosed cell-surface proteins that escape MVB sorting. We wanted to examine if loss of this next tier of QC in mutants already compromised to respond to heat stress, would further aggravate the defects in cellular fitness. To test this, we generated mutants lacking Art1 as well as Ssh4 and Ear1 and compared the single or combination mutants for growth. The *art1*Δ mutant displayed slower growth when incubated at 34°C, as reported earlier (Zhao et al., 2013). Although *ssh4*Δ and *ear1*Δ single or double mutants alone did not exhibit any observable fitness defect at 34°C, their deletion in an *art1*Δ background resulted in a significant decrease in cellular fitness (Fig. 8 A). Lack of Rsp5 adaptors at all steps of the endocytic pathway is likely to cause an accumulation of PM proteins at the cell surface as well as intracellularly, resulting in proteotoxic stress. The lysine permease Lyp1 was previously reported to be particularly

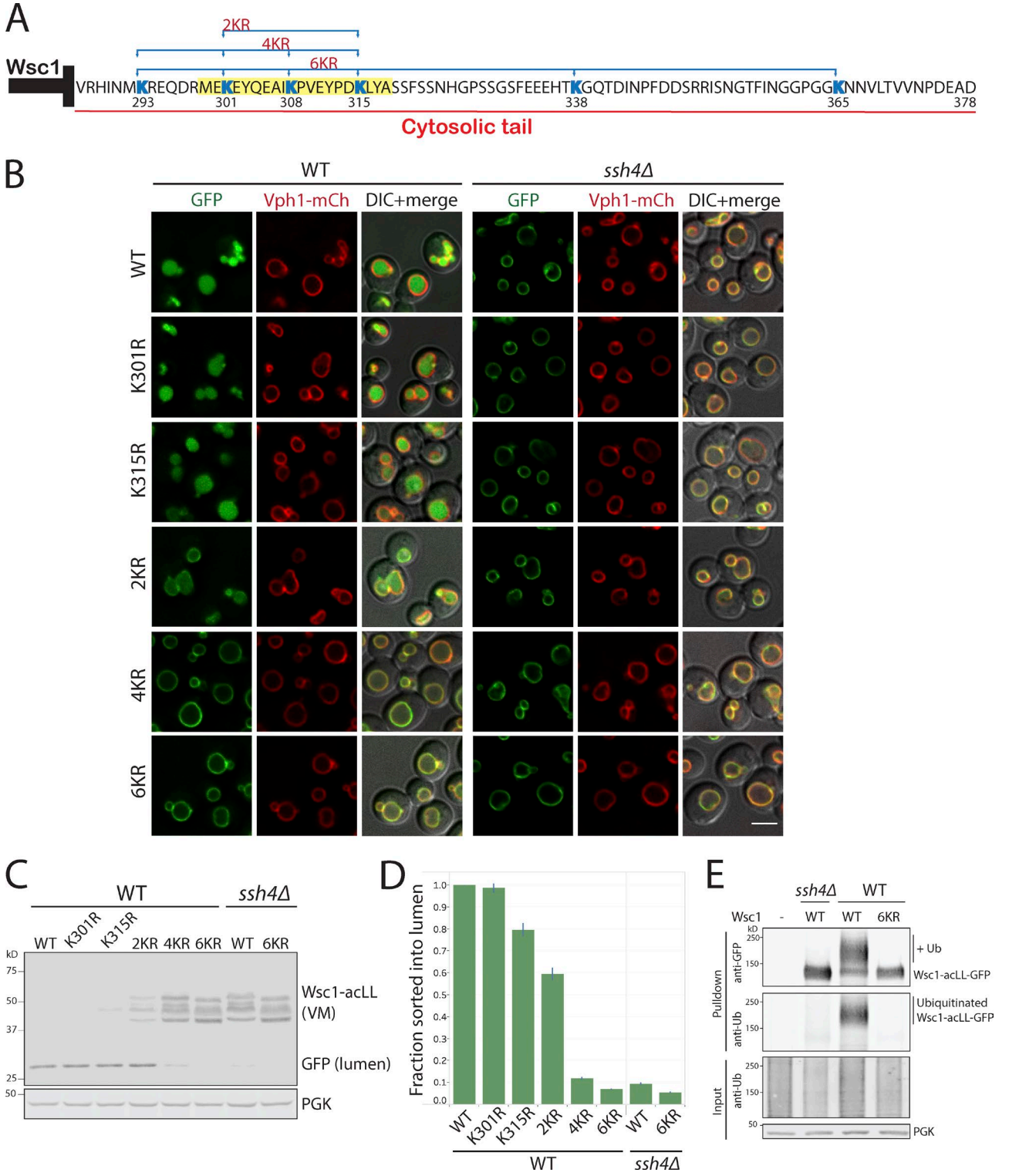

Figure 5. **The Ssh4–Rsp5 complex can target multiple accessible cytosolic lysines. (A)** Sequence of the 93-aa cytosolic tail of Wsc1 with the lysines highlighted in blue. The position of the lysine residues and the combination mutants are indicated below and above the sequence, respectively. The 20-aa sequence in the Wsc1$^{286–318}$ mutant required for sorting is highlighted in yellow. **(B)** WT and *ssh4*Δ mutant expressing Wsc1-acLL-GFP with K>R mutation at single (K301 or K315) or simultaneous mutations at two (2KR; K301R and K315R), four (4KR; K293R, K301R, K308R, and K315R), or all six (6KR; K293R, K301R, K308R, K315R, K338R, and K365R) cytosolic lysines. Scale bar: 2.5 µm. VM marker, Vph1-mCherry. **(C)** Immunoblot analysis on WT and *ssh4*Δ extracts expressing the mutants described in B. **(D)** Quantitation of three replicates of immunoblot analyses described in C. The fraction of Wsc1-acLL-GFP sorted into the lumen refers to the ratio of the processed GFP to the total reporter levels normalized to WT. Error bars indicate standard error of the measurements. **(E)** Immunoprecipitation followed by Western blot analysis of cells expressing WT or Wsc1$^{6K>R}$-acLL-GFP in WT or *ssh4*Δ cells (also lacking Doa4, Pep4, and Prb1 to stabilize ubiquitinated species).

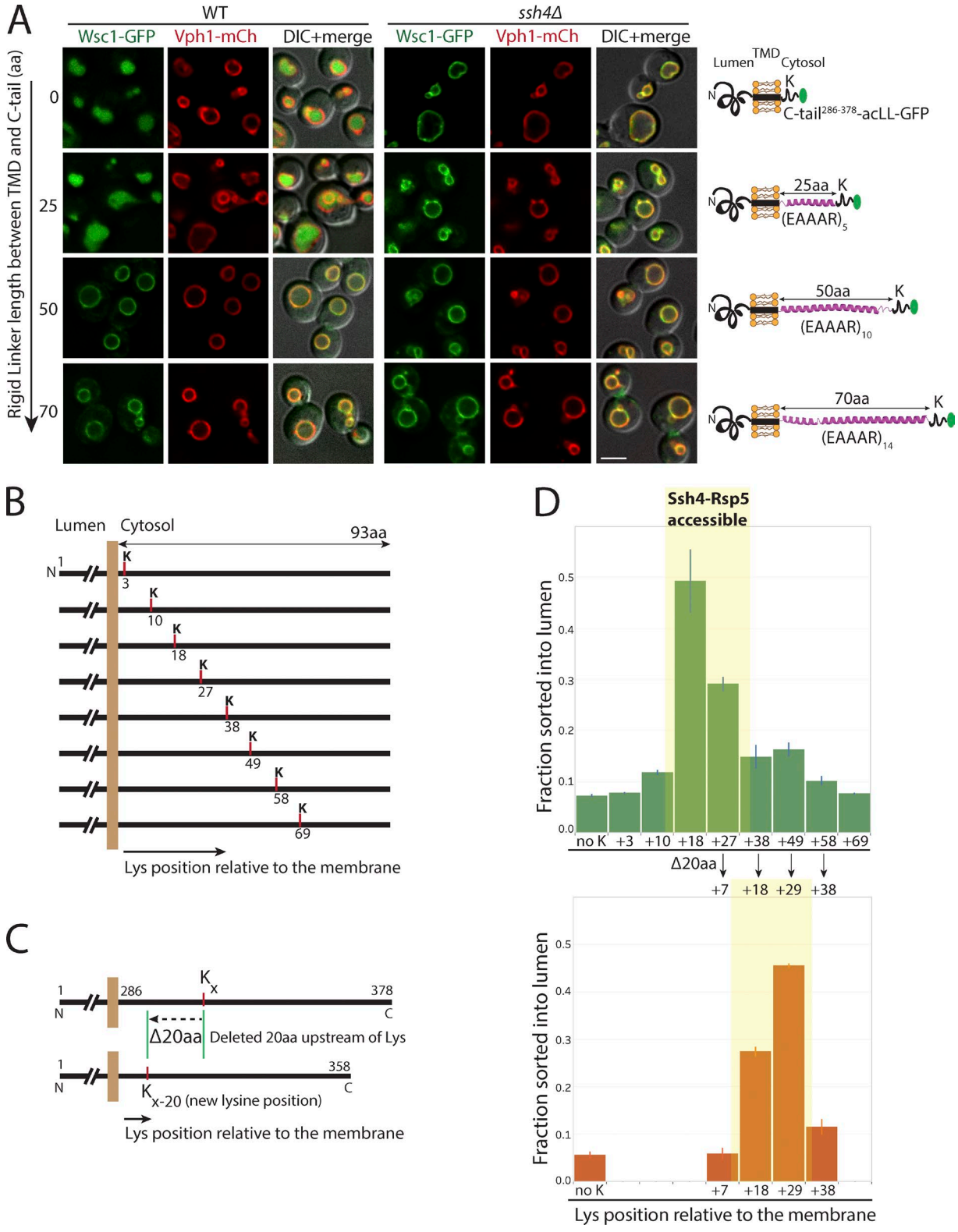

Figure 6. **Lysine positioning relative to the membrane is critical for Ssh4–Rsp5–mediated recognition at the VM. (A)** Fluorescence microscopy of WT and *ssh4Δ* mutant cells expressing Wsc1-acLL-GFP with a rigid α-helical linker containing repeats of $(EAAAR)_n$ of indicated lengths between the TMD and the cytosolic tail. Scale bar: 2.5 µm. VM marker, Vph1-mCherry. **(B)** Schematic for $Wsc1^{6K>R}$-acLL-GFP with only one lysine added at the indicated positions in the cytosolic tail of Wsc1. **(C)** Schematic describing the deletion of 20 aa upstream of the available lysine shifting the lysine position closer to the membrane. **(D)** Quantitation of the fraction sorted into the lumen from three replicates of immunoblot analyses on extracts prepared from WT cells expressing $Wsc1^{6K>R}$-acLL-GFP (no K) or variants described in B (top) and C (bottom). Error bars indicate standard error of the measurements.

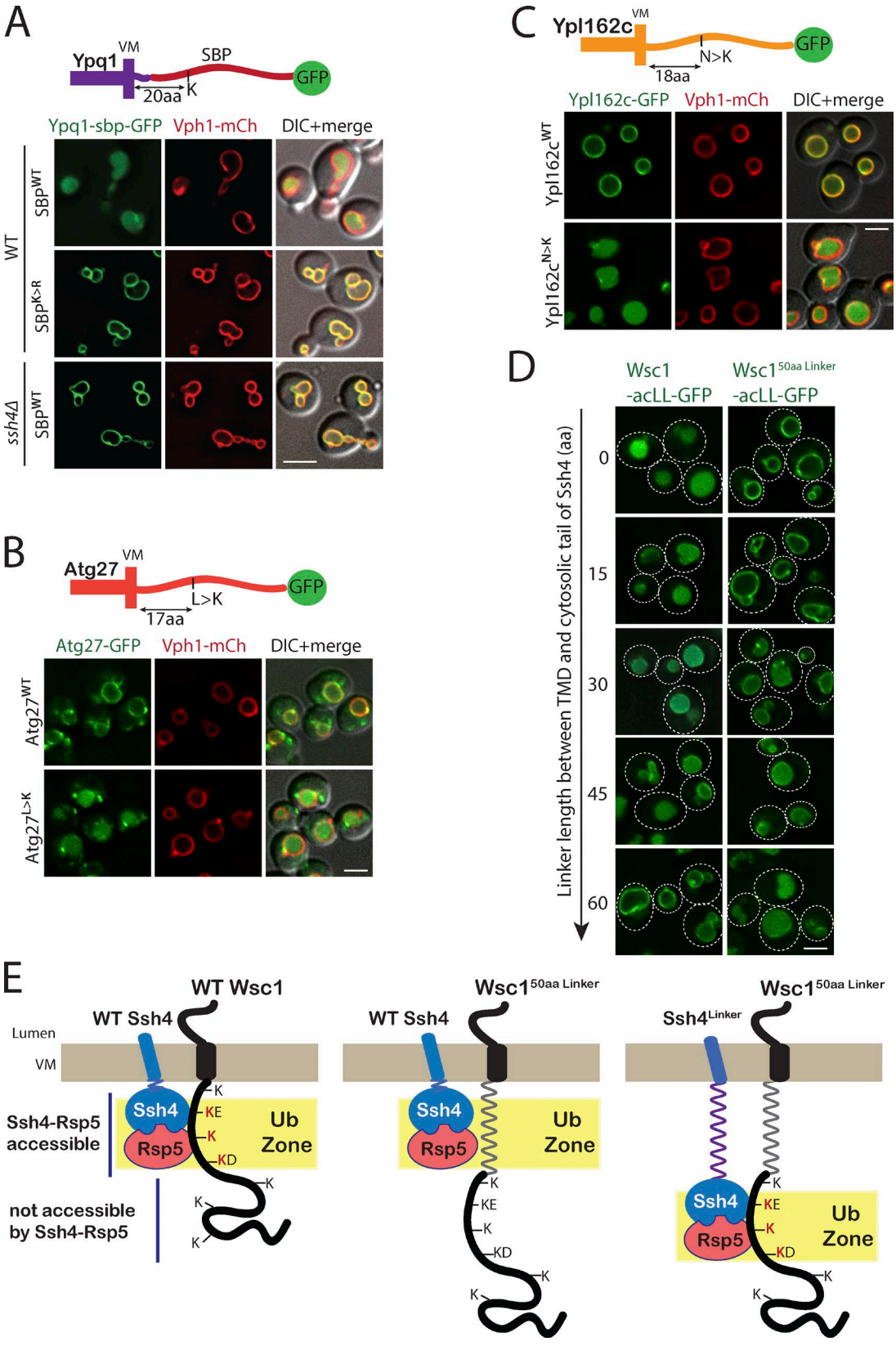

Figure 7. **Addition of a lysine to the ubiquitination zone results in constitutive degradation of stable VM proteins. (A)** Fluorescence microscopy of WT and *ssh4*Δ mutant cells expressing Ypq1-SBP^{WT} or SBP$^{K>R}$-GFP. Scale bar: 2 µm. VM marker, Vph1-mCherry. **(B)** WT cells expressing GFP tagged Atg27^{WT} or Atg27$^{L>K}$ mutant. **(C)** WT cells expressing GFP tagged Ypl162c^{WT} or Ypl162c$^{N>K}$. **(D)** WT cells expressing Wsc1-acLL-GFP or Wsc1^{50aaLinker}-acLL-GFP and Ssh4 with linkers of varying lengths (15, 30, 45, and 60 aa) between the TMD and the cytosolic domain. Dashed lines indicate the cell periphery. Scale bar: 2.5 µm. VM marker, Vph1-mCherry. **(E)** Model for Ssh4–Rsp5–mediated recognition of cytosolic lysines in the ubiquitination zone in cargos at the VM.

susceptible to misfolding upon heat stress and its accumulation on the cell surface in an *art1*Δ mutant was reported to be a major determinant of the reduced fitness upon heat stress (Zhao et al., 2013). Indeed, Lyp1-GFP accumulated at the cell surface as well as on the VM in the *art1*Δ *ssh4Δ ear1*Δ triple mutant (Fig. 8 B). Titration of Lyp1 expression using different promoters to manipulate Lyp1 accumulation directly correlated with the temperature sensitivity of the *art1*Δ mutant (Zhao et al., 2013). We reasoned that overexpression of Lyp1 in the *art1*Δ *ssh4Δ ear1*Δ triple mutant should further distress the already imbalanced QC, resulting in a stronger toxicity phenotype. To test this, we titrated Lyp1 levels using weak (P_{CPY}) or strong (P_{ADH} and P_{GPD}) expression promoters as previously demonstrated (Zhao et al., 2013). Indeed, the *art1*Δ *ssh4*Δ *ear1*Δ triple mutant was particularly sensitive to the toxicity caused by Lyp1 accumulation even at 26°C (Fig. 8 C). This observation was also supported by the toxicity due to overexpression of several PM proteins in the triple mutant (data not shown). To measure the effect of the loss of surveillance along the endocytic pathway on cellular integrity, we employed the polar fluorescent vital dye propidium iodide (PI), which is membrane impermeant in healthy cells. However, loss of PM integrity results in uptake of PI that can be monitored by increased fluorescence. We employed flow cytometry to quantitatively analyze PI staining before and after exposure to heat stress for 3 h at 40°C. WT cells exhibited negligible PI staining at 26°C and weak staining after 3 h at 40°C (Fig. 8 D). As expected, *end3*Δ mutant with strongly abrogated endocytosis exhibited significant PI staining even at 26°C, that rose to ∼80% after heat stress. In agreement with our observations on growth, when the *art1*Δ mutant is combined with loss of intracellular adaptors, it resulted in a striking increase in PI staining, indicating an increased propensity for cell lysis upon stress (Fig. 8 D). These observations suggest that the absence of the multitier surveillance provided by cell-surface and intracellular adaptors can cause a cumulative impairment in the timely clearance or aberrant accumulation of proteins in the PM and intracellular membranes. This accumulation can potentially compromise organelle identities and aberrantly activate cellular signaling paradigms. Overall, our findings highlight the importance of cooperation between successive layers of protein QC in the endocytic system (Fig. 9).

Discussion

Sequential endocytic Ub-ligase QC checkpoints ensure proteostasis

Subcellular compartmentalization of proteins enables functional specialization of organelles. Continuous surveillance by organelle-specific QC systems is critical for routine housekeeping, to protect organelles from damage and to prevent disease states. While QC systems are conventionally thought to survey protein misfolding, our work emphasizes the importance of QC mechanisms to also prevent accumulation of proteins foreign to the organelle. Organelles are highly dynamic, and proteins (particularly integral membrane proteins) traffic from one organelle to another via the secretory and endocytic pathways. Mistargeting or inappropriate accumulation of membrane proteins in the wrong organelle can lead to loss of proper organelle identity as well as membrane damage. Constant monitoring by QC systems acting in sequential organelles ensure maintenance of appropriate organelle composition and function. In the secretory pathway, the ERAD machinery provides a key mechanism for identification and clearance of misfolded proteins (Berner et al., 2018); however, post-ER pathways for protein QC at the Golgi have also been reported. Misfolded proteins that escape, saturate, or fail to be recognized by ERAD mechanisms traffic to the Golgi, where specific receptors can recognize and route them back to the ER, or Golgi-based E3 ligases can specifically ubiquitinate them, which redirects them to the endosomal/MVB system for degradation in the vacuole (Chang and Fink, 1995; Li et al., 1999; Arvan et al., 2002; Pizzirusso and Chang, 2004; Wang et al., 2011).

Our work highlights the importance of sequential layers of membrane protein surveillance in the endocytic system. The quality and quantity of membrane proteins at the cell surface is assessed by the ART–Rsp5 network which plays a critical role in Ub-dependent down-regulation of PM proteins in response to changes in the environment (Lin et al., 2008; Lauwers et al., 2010; Becuwe et al., 2012; Zhao et al., 2013). Several PM proteins are also endocytosed in a Ub-independent manner (eg, Wsc1 and Snc1), and the decision to target these proteins for degradation initiates intracellularly. Multiple intracellular PY motif–containing adaptors (Bul1/Bul2, Bsd2, Tre1/Tre2, Sna3, Ear1, and Ssh4) also recruit Rsp5 and target membrane proteins for ubiquitination (Hettema et al., 2004; Léon et al., 2008; O'Donnell, 2012). Ear1 and Ssh4 were previously reported to be required for biosynthetic MVB sorting of Gap1 and Sit1 along the VPS pathway, as well as for endocytosed Fur4 (Léon et al., 2008). Our current work demonstrates that Ear1 and Ssh4 perform a crucial second tier of QC for a broad spectrum of endocytosed cargos. Ear1 recruits Rsp5 to the endosome to provide the first intracellular checkpoint. Cargo that escapes MVB sorting or is not captured by recycling complexes at the endosome gets delivered to the VM upon fusion of the endosome with the vacuole. Here, it encounters the Ssh4–Rsp5 E3 ligase complex that ensures these cargos do not accumulate on the VM. Thus ARTs, Ear1 and Ssh4 act as successive checkpoints in the endocytic pathway to ensure that multiple endocytosed PM proteins (whether ubiquitinated at the PM or not) are delivered to the vacuole lumen for degradation (Fig. 9). The stage-specific organization of distinct adaptor–Rsp5 Ub-ligase complexes ensures smooth endocytic function and prevents unnecessary accumulation of membrane proteins. This orchestrated hierarchy of organelle QC becomes especially important in conditions of stress when it is critical to remove misfolded proteins to maintain cellular integrity (Fig. 8).

Why would such a system be required for proteins that are already ubiquitinated at the PM for endocytosis? Most QC complexes contain competing ubiquitination as well as deubiquitination activities, and the fate of the target protein is determined by a balance of these antagonizing reactions (Kee et al., 2005; Ren et al., 2007; Zhang et al., 2013; Piper et al., 2014). Regulation of these competing activities has been shown to dictate the fate of Jen1 in yeast and β2-adrenergic receptor in mammalian cells (Berthouze et al., 2009; Becuwe and Léon, 2014). Inappropriate deubiquitination or inefficient ESCRT mediated MVB sorting introduces the need to continually monitor and reubiquitinate QC cargos throughout the endocytic pathway.

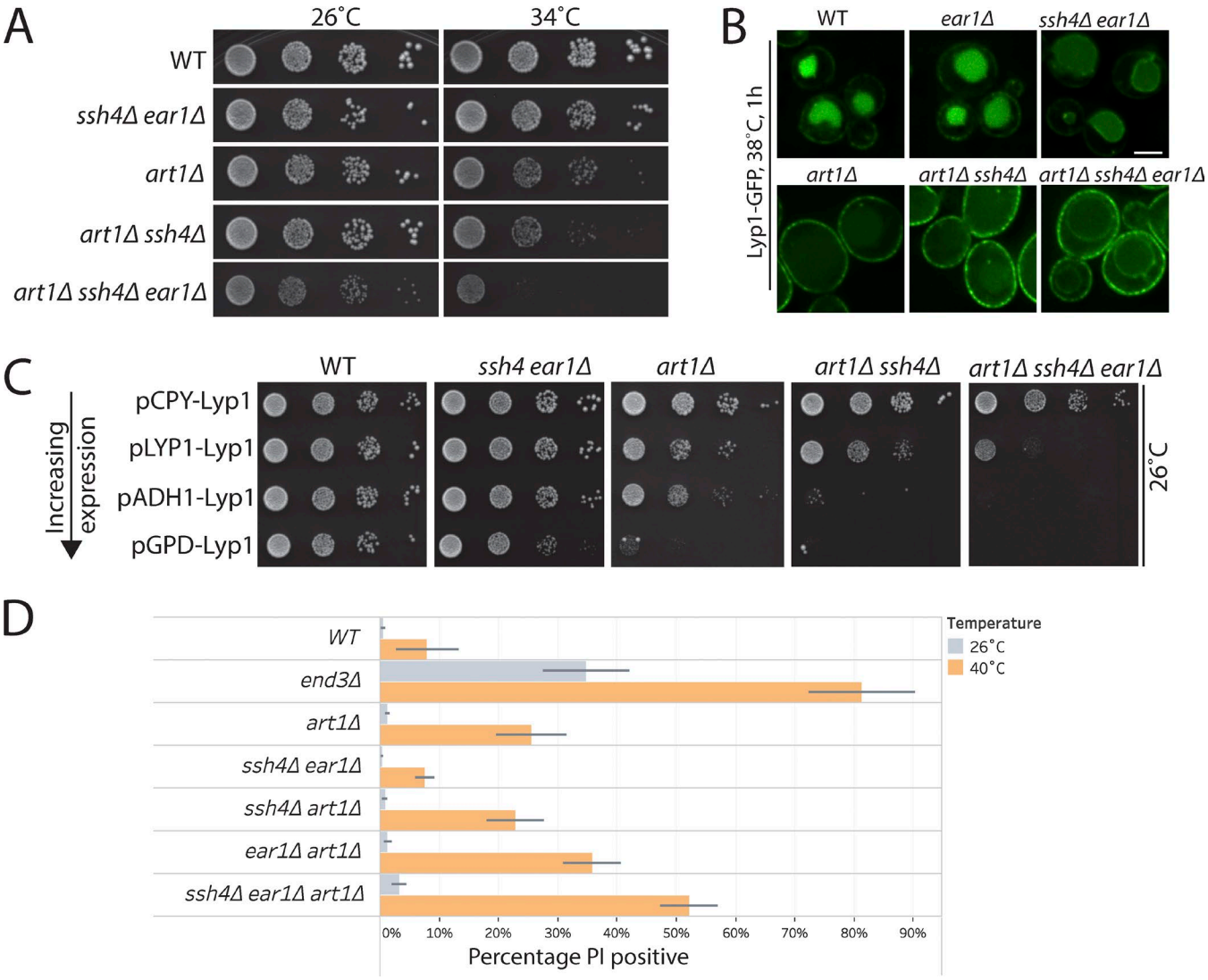

Figure 8. **Intracellular and cell surface QC systems cooperatively ensure maintenance of proteostasis. (A)** 10-fold serial dilutions of WT or *art1Δ*, *ssh4Δ ear1Δ*, *art1Δ ssh4Δ*, and *art1Δ ssh4Δ ear1Δ* mutants spotted on synthetic complete medium plates and incubated at 26°C and 34°C for 3 d. **(B)** WT or *ear1Δ*, *ssh4Δ ear1Δ*, *art1Δ*, *art1Δ ssh4Δ*, and *art1Δ ssh4Δ ear1Δ* mutants expressing Lyp1-GFP exposed to heat stress at 38°C for 1 h before imaging. Scale bar: 2.5 µm. **(C)** Growth assay to compare the effect of Lyp1 overexpression from P_{LYP1}, weak promoter (P_{CPY}), or strong promoter (P_{ADH} and P_{GPD}) in WT or *ssh4Δ ear1Δ*, *art1Δ*, *art1Δ ssh4Δ*, and *art1Δ ssh4Δ ear1Δ* mutants. Mid-log phase cultures were spotted on synthetic medium lacking uracil and incubated at 26°C for 3–5 d. **(D)** Flow cytometry–based cell integrity analysis measured by PI staining of WT, *end3Δ*, *art1Δ*, *art1Δ ssh4Δ*, *art1Δ ear1Δ*, *ssh4Δ ear1Δ*, and *art1Δ ssh4Δ ear1Δ* mutants at 26°C or upon shift to 40°C for 3 h. The bar graphs represent the average PI-positive fraction, and error bars indicate standard error of the measurements.

A fail-safe mechanism for removal of mislocalized proteins from the VM

The challenge to studying sequential recognition lies in being able to study each step in isolation. Our strategy of misdirecting PM proteins to the VM de novo by the addition of AP-3 adaptor recognition motif successfully overcomes this handicap. The trafficking of the PM-acLL reporters directly from the Golgi to the VM via the AP-3 pathway bypasses recognition by adaptors along the MVB route, thus allowing separation of the Ub-ligase recognition step at the PM and the endosome from the surveillance step at the VM by Ssh4. Our findings using these mistargeted reporters also demonstrate that the recognition at the VM is quite robust and selective. Despite the presence of several Ub ligases at the VM such as Tul1 and Pib1 (Shin et al., 2001; Li et al., 2015a), as well as other Rsp5 adaptors such as Rcr2 (Kota et al., 2007), only the Ssh4–Rsp5 complex was able to recognize the mistargeted cargos for ubiquitination and degradation. This strongly argues that different Ub ligases at the VM likely recognize a distinct subset of cargo features to provide maximal coverage for VM surveillance. And yet, within that subset, the Ssh4–Rsp5 complex is able to recognize seemingly diverse cargos with variable TMDs and no obvious shared sequence motif that is conserved in either lumenal or cytosolic domains.

A particularly interesting and elusive question for all QC systems is how they distinguish between different candidate membrane protein targets; how is specificity encoded in these systems? At the PM, changes in nutrient availability or environmental stress are thought to cause conformational changes exposing an amino acid sequence motif or a "degron" recognized by specific Rsp5 adaptors (Zhao et al., 2013; Piper et al., 2014; Guiney

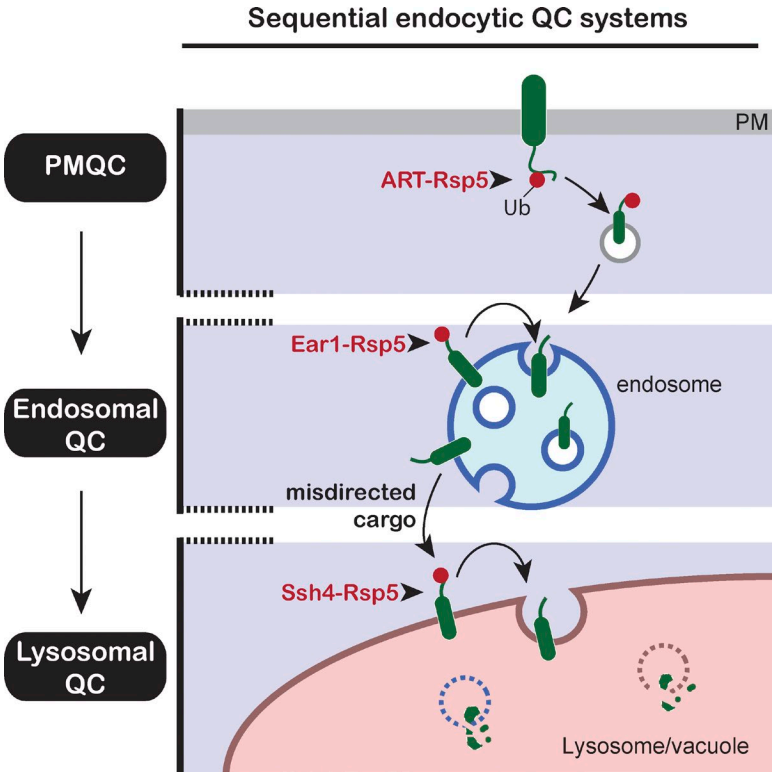

Figure 9. **Tiered surveillance structure of the endocytic QC systems.** The ART–Rsp5 network monitors Ub-dependent endocytic cargos at the cell surface (PMQC). Cargos that escape ubiquitination or MVB sorting are exposed to endosomal QC or are delivered to the VM upon fusion of the endosome with the vacuole (analogous to lysosomes in higher eukaryotes). The Ssh4–Rsp5 E3 ligase complex provides the final clearance mechanism to ensure removal of aberrant membrane proteins (lysosomal QC).

et al., 2016). We show that the Ssh4–Rsp5 checkpoint lacks a conventional degron requirement and instead provides a fail-safe mechanism that enables the degradation of a far broader range of substrates. Using the Wsc1-acLL-GFP reporter, we find that Ssh4–Rsp5 can modify several accessible cytosolic lysines appropriately positioned in a narrow window relative to the membrane. We put the spacing requirement to test by adding linkers in the cargo as well as Ssh4. This is reminiscent of the mechanism employed by the Cullin-RING ligase in SCF complex when it binds the p27 target, where the ligase can access and modify multiple lysines in a limited area referred to as the ubiquitination zone (Mattiroli and Sixma, 2014). Recent structural analysis of Rsp5 also provided evidence that the ligase activity of Rsp5 is spatially restricted, and a joint function of the N and C lobes of Rsp5 is required for catalysis (Kamadurai et al., 2013). Our observation for Ssh4–Rsp5–mediated surveillance favors a model in which the membrane-tethered Ssh4–Rsp5 complex transiently interacts with many potential targets on the VM via weak interactions, which is stabilized only when the recognition of accessible lysines allows Rsp5 catalyzed ubiquitination of the target. Additionally, membrane-bound Ssh4 may facilitate the proper orientation of the catalytic site of Rsp5 to allow it to only modify exposed lysines in a restricted distance from the membrane. The specificity is thus contributed by the spatial restriction of lysines in the cargo and the compartmental restriction of the Ub ligase adaptor complex.

The seemingly nonspecific mechanism of recognition also raises the question of how resident VM proteins are protected from the wrath of Ssh4–Rsp5. Certainly, most VM proteins contain one or more lysines in their cytosolic tails. A probable explanation may be that modifiable lysines are inaccessible to Ssh4–Rsp5 because they are hidden within domain folds or by interactions with other proteins. However, conformational changes or dissociation of interacting partners may make them susceptible to ubiquitination by Ssh4–Rsp5. Mistargeted PM cargos in the new membrane environment of the VM, on the other hand, may also undergo conformational changes that result in exposure of the target lysines accessible to the Ssh4–Rsp5 complex.

Ssh4 and Ear1 differ from PM-based adaptors of Rsp5 (ARTs) in distinct ways. Ssh4 and Ear1 are integral membrane proteins tethered to their target organelle, while the ARTs are cytosolic proteins recruited to the PM upon specific cues. The integral membrane adaptors have extended access to the targets in their vicinity, potentially allowing weaker interactions to facilitate degradation fates. Additionally, in contrast to cytosolic adaptors, all the intracellular membrane adaptors of Rsp5 studied so far (Bsd2, Tre1/Tre2, and Ear1/Ssh4) are sorted into the vacuole lumen along with the cargo, thus acting as "suicide adaptors," allowing a built-in mechanism to control Rsp5 availability (Hettema et al., 2004; Léon et al., 2008). Furthermore, Ssh4's ability to recruit Rsp5 and efficiently ubiquitinate cargos may be regulated by posttranslational modifications such as phosphorylation and ubiquitination of Ssh4 and will need further exploration. Although Ssh4 or Ear1 do not appear to have a direct human homologue, the SPRY/B30.2 domain present in Ssh4 and Ear1 is a common protein interaction adaptor module in higher eukaryotes, and ∼45% of the human SPRY-containing proteins (total of >100) are E3 Ub ligases (Perfetto et al., 2013). Furthermore, transmembrane lysosomal E3 Ub ligases such as RNF152 and RNF167 have also been identified (Nakamura, 2011; Deng et al., 2015).

Finally, why is such an orchestrated hierarchy of Ub-ligase checkpoints important? We show that attentive housekeeping

by a network of surveillance factors in sequential compartments throughout the endocytic system keeps a check on upstream errors and, more importantly, prevents the accumulation of nonfunctional proteins in undesired locations or the aberrant activation of critical cellular signaling cascades. The interdependence of these clearance systems manifests acutely in conditions of cellular stress, when one or more PQC systems are overburdened or when growth conditions are unfavorable. Taken together, we present a model where PY motif–containing adaptors throughout the endocytic system (ARTs at the PM, Ear1 at the endosome, and Ssh4 at the VM) recruit Rsp5 to ensure rapid down-regulation of membrane proteins from the cell surface as well as organelle membranes. The loss of this multitier clearance system results in a toxic buildup of undesired membrane proteins at the cell surface as well as on the terminal vacuolar membrane.

Materials and methods

Yeast strains and plasmids

All yeast strains and plasmids were constructed using standard techniques and are described in Tables S1 and S2.

Yeast growth assays

For yeast dilution spot assays, mid-log phase cultures were grown at 26°C in synthetic complete or selective media. Cells were diluted to 0.3 OD in 200 µl water, and 10-fold serial dilutions were spotted on growth media and incubated at the indicated temperatures for 3–5 d.

Fluorescence microscopy

Yeast cells expressing fluorescence fusion proteins were grown to mid-log phase in appropriate synthetic media at 26°C, unless otherwise indicated. For imaging Mup1-GFP or Mup1-acLL-GFP, cells were grown in media lacking methionine at 26°C. To induce Mup1-GFP endocytosis, methionine was added to a final concentration of 20 µg/ml for 90 min. 0.5 OD_{600} equivalent of cells was harvested and washed with water before imaging. Cells were applied to a clean glass slide under a coverslip and imaged at room temperature. Microscopy was performed using a DeltaVision Elite system (GE Healthcare Life Sciences) equipped with an Olympus IX-71 inverted microscope, DV Elite complementary metal-oxide semiconductor camera, a 100×/1.4 NA oil objective, and a DV Light SSI 7 Color illumination system with Live Cell Speed Option with DV Elite filter sets (FITC and mCherry channels for GFP and mCherry, respectively). Image acquisition and deconvolution (conservative setting; five cycles) were performed using DeltaVision software softWoRx 6.5.2 (Applied Precision). Images were adjusted for brightness and contrast with identical processing of all images within a single figure panel. Images were processed in ImageJ and assembled in Adobe Illustrator CS6. Each image shown is a single focal plane. Lyp1-GFP accumulation at the VM in WT and *ssh4*Δ *ear1*Δ mutant was quantified in Python 3.6.1. VMs were detected using the VM marker Vph1-mCherry by Otsu thresholding (using scikit-image package). Images were background corrected, and GFP signal was measured in the total vacuole (VM and the lumen) and on the VM. A total of 443 WT vacuoles and 309 mutant vacuoles were scored for the analysis. Accumulation on the VM was calculated as the ratio of median VM signal to the median total vacuolar GFP signal. Percent accumulation for mutant was calculated by normalizing to WT.

Protein extraction and Western blotting

Yeast cells expressing epitope-tagged proteins were grown to mid-log phase in synthetic media at 26°C. 5–7 OD_{600} equivalent of cells was harvested and incubated in 10% TCA on ice for 3 h. The cells were washed with acetone, lysed by beating with glass beads in 80 µl of 2× urea buffer (50 mM Tris-HCl, pH 7.5, 8 M urea, 2% SDS, and 1 mM EDTA) for 5 min at room temperature, and incubated at 42°C for 10 min. 80 µl of 2× sample buffer (150 mM Tris-Cl, pH 6.8, 8 M urea, 8% SDS, 24% glycerol, 100 mM DTT, and bromophenol blue) supplemented with 100 mM DTT was then added, and samples were again vortexed for 5 min followed by incubation at 42°C for 10 min. Samples were centrifuged for 3 min at 21,000 *g* on a tabletop centrifuge. Protein samples were resolved on a 10% SDS-polyacrylamide gel and transferred to nitrocellulose membrane (0.45 µm; GE Healthcare) at 4°C via wet transfer in transfer buffer (25 mM Tris, 192 mM glycine, 20% vol/vol methanol, and 0.006% SDS) at 100 V for 2 h. Membranes were blocked with 5% fat-free milk in 1× TBST (20 mM Tris-Cl, pH 7.5, 150 mM NaCl, and 0.05% Tween-20) for 30 min at room temperature and blotted with indicated primary antibodies diluted in 1× TBST for 3 h at room temperature or overnight at 4°C, washed three times with 1× TBST (10 min each time), and incubated with secondary antibodies diluted in 1× TBST for 1 h at room temperature. Membranes were washed three times with 1× TBST and then scanned using an Odyssey CLx imaging system and analyzed using the Image Studio Lite 4.0.21 software (LI-COR Biosciences). Images were assembled in Adobe Illustrator CS6. Quantitation was performed using three biological replicates of immunoblot analyses. The fraction of reporter sorted into the lumen refers to the ratio of the processed GFP to the total reporter levels normalized to the loading control. The ratios were normalized to WT for ease of comparison. For Mup1 degradation assay in Fig. 3 E, full-length Mup1-acLL-GFP and free GFP were detected with rabbit polyclonal anti-GFP antibody on a single membrane and brightness and contrast were adjusted separately due to differences in transfer efficiency.

The following antibodies and dilutions were used: rabbit polyclonal anti-GFP (1:5,000; TP401; Torrey Pines Biolabs), mouse monoclonal anti-PGK (1:5,000; 22C5D8; Molecular Probes), mouse monoclonal anti-Ub (1:1,000; MAB1510; Millipore Sigma), 800CW goat anti-rabbit (1:10,000; 926-32211; LI-COR Biosciences), and 680LT goat anti-mouse (1:10,000; 926-68021; LI-COR Biosciences).

Immunoprecipitation and ubiquitination assay

Ubiquitination assays were performed using cells also lacking Doa4 (the key deubiquitinating enzyme of the endomembrane system, to stabilize ubiquitinated species), as well as the vacuolar hydrolases Pep4 and Prb1 (to block degradation of the ubiquitinated Wsc1-acLL-GFP in the vacuole lumen), and overexpressing Ub from a 2-µm vector. Cells were grown to OD_{600} ∼0.5 in 200–250 ml synthetic growth media and harvested on ice. Cells were washed and resuspended in lysis buffer (20 mM Tris, pH 7.5,

0.5 mM EDTA, pH 8.0, 200 mM NaCl, 10% glycerol, 1 mM PMSF, 10 mM *N*-ethylmaleimide, and 1× Roche cOmplete Protease Inhibitor Tablet/50 ml). Cell extracts were prepared by glass-bead beating for five cycles of 1 min vortexing with 1 min breaks on ice. Membranes were solubilized by nutating for 30 min at 4°C after addition of Triton X-100 to 0.1% final concentration. Crude extracts were clarified by centrifugation at 16,000 *g* for 10 min at 4°C. The cleared lysate was incubated with 25 µl GFP-nanobody resin (Guiney et al., 2016) at 4°C for 4 h. The resin was washed three times with lysis buffer containing 0.02% Triton X-100, and bound proteins were eluted by addition of 50 µl 2× sample buffer, followed by incubation at 42°C for 10 min. The resulting eluates were analyzed by Western blotting.

PM integrity assay

Yeast strains were grown to early-log phase (~0.2 OD_{600}) in synthetic media at 26°C and split in half, and one half was shifted to 40°C for 3 h. 0.25 OD_{600} equivalent of cells was pelleted and resuspended in PBST (PBS with 0.01% Tween-20) and cells were stained with 1 µl of 20 mM PI (Sigma; in DMSO) for 15 min at room temperature. Cells were then washed twice with 1 ml PBS. and 150,000–200,000 cells for each condition were analyzed using an Accuri C6 flow cytometer. Three biological replicates were analyzed for each sample.

Online supplemental material

Fig. S1 shows that multiple PM cargos endocytosed via Ub-dependent and Ub-independent mechanisms accumulate on the VM in *ssh4*Δ *ear1*Δ mutant. Fig. S2 shows that vacuolar lumenal localization of Mup1-acLL-GFP is independent of endocytosis. Fig. S3 shows that acidic dileucine-tagged cargos are blocked on the VM in *vps4*Δ mutants defective for ESCRT function. Fig. S4 shows the localization and stability of Wsc1-acLL-GFP mutants containing only one lysine at the indicated position in the cytosolic tail. Table S1 is a list of yeast strains used in this study. Table S2 is a list of plasmids used in this study.

Acknowledgments

We thank Evan Guiney, Matthew Baile, Sho Suzuki, and Sid Banerjee for feedback on the manuscript and all members of the Emr laboratory for helpful discussions. We also thank Sid Banerjee for help with Python analysis and Jonathan Weng for cloning assistance.

This work was supported by a Cornell University research grant to S.D. Emr.

The authors declare no competing financial interests.

Author contributions: Conceptualization: R. Sardana and S.D. Emr; Methodology: R. Sardana; Investigation: R. Sardana and L. Zhu; Validation: R. Sardana; Formal Analysis: R. Sardana; Visualization: R. Sardana; Writing – Original Draft: R. Sardana; Writing – Review & Editing: R. Sardana and S.D. Emr; Supervision: S.D. Emr; Funding Acquisition: S.D. Emr.

Submitted: 14 June 2018
Revised: 6 September 2018
Accepted: 1 October 2018

References

Amerik, A.Y., J. Nowak, S. Swaminathan, and M. Hochstrasser. 2000. The Doa4 deubiquitinating enzyme is functionally linked to the vacuolar protein-sorting and endocytic pathways. *Mol. Biol. Cell.* 11:3365–3380. https://doi.org/10.1091/mbc.11.10.3365

Arvan, P., X. Zhao, J. Ramos-Castaneda, and A. Chang. 2002. Secretory pathway quality control operating in Golgi, plasmalemmal, and endosomal systems. *Traffic.* 3:771–780. https://doi.org/10.1034/j.1600-0854.2002.31102.x

Becuwe, M., and S. Léon. 2014. Integrated control of transporter endocytosis and recycling by the arrestin-related protein Rod1 and the ubiquitin ligase Rsp5. *eLife.* 3:e03307. https://doi.org/10.7554/eLife.03307

Becuwe, M., A. Herrador, R. Haguenauer-Tsapis, O. Vincent, and S. Léon. 2012. Ubiquitin-mediated regulation of endocytosis by proteins of the arrestin family. *Biochem. Res. Int.* 2012:242764. https://doi.org/10.1155/2012/242764

Belgareh-Touzé, N., S. Léon, Z. Erpapazoglou, M. Stawiecka-Mirota, D. Urban-Grimal, and R. Haguenauer-Tsapis. 2008. Versatile role of the yeast ubiquitin ligase Rsp5p in intracellular trafficking. *Biochem. Soc. Trans.* 36:791–796. https://doi.org/10.1042/BST0360791

Bénédetti, H., S. Raths, F. Crausaz, and H. Riezman. 1994. The END3 gene encodes a protein that is required for the internalization step of endocytosis and for actin cytoskeleton organization in yeast. *Mol. Biol. Cell.* 5:1023–1037. https://doi.org/10.1091/mbc.5.9.1023

Berner, N., K.-R. Reutter, and D.H. Wolf. 2018. Protein Quality Control of the Endoplasmic Reticulum and Ubiquitin-Proteasome-Triggered Degradation of Aberrant Proteins: Yeast Pioneers the Path. *Annu. Rev. Biochem.* 87:751–782. https://doi.org/10.1146/annurev-biochem-062917-012749

Berthouze, M., V. Venkataramanan, Y. Li, and S.K. Shenoy. 2009. The deubiquitinases USP33 and USP20 coordinate beta2 adrenergic receptor recycling and resensitization. *EMBO J.* 28:1684–1696. https://doi.org/10.1038/emboj.2009.128

Chang, A., and G.R. Fink. 1995. Targeting of the yeast plasma membrane [H+] ATPase: a novel gene AST1 prevents mislocalization of mutant ATPase to the vacuole. *J. Cell Biol.* 128:39–49. https://doi.org/10.1083/jcb.128.1.39

Cowles, C.R., G. Odorizzi, G.S. Payne, and S.D. Emr. 1997. The AP-3 adaptor complex is essential for cargo-selective transport to the yeast vacuole. *Cell.* 91:109–118. https://doi.org/10.1016/S0092-8674(01)80013-1

Deng, L., C. Jiang, L. Chen, J. Jin, J. Wei, L. Zhao, M. Chen, W. Pan, Y. Xu, H. Chu, et al. 2015. The ubiquitination of rag A GTPase by RNF152 negatively regulates mTORC1 activation. *Mol. Cell.* 58:804–818. https://doi.org/10.1016/j.molcel.2015.03.033

Fisk, H.A., and M.P. Yaffe. 1999. A role for ubiquitination in mitochondrial inheritance in Saccharomyces cerevisiae. *J. Cell Biol.* 145:1199–1208. https://doi.org/10.1083/jcb.145.6.1199

Guiney, E.L., T. Klecker, and S.D. Emr. 2016. Identification of the endocytic sorting signal recognized by the Art1-Rsp5 ubiquitin ligase complex. *Mol. Biol. Cell.* 27:4043–4054. https://doi.org/10.1091/mbc.e16-08-0570

Heinisch, J.J., V. Dupres, S. Wilk, A. Jendretzki, and Y.F. Dufrêne. 2010. Single-molecule atomic force microscopy reveals clustering of the yeast plasma-membrane sensor Wsc1. *PLoS One.* 5:e11104. https://doi.org/10.1371/journal.pone.0011104

Henne, W.M., H. Stenmark, and S.D. Emr. 2013. Molecular mechanisms of the membrane sculpting ESCRT pathway. *Cold Spring Harb. Perspect. Biol.* 5:a016766. https://doi.org/10.1101/cshperspect.a016766

Hettema, E.H., M.J. Lewis, M.W. Black, and H.R.B. Pelham. 2003. Retromer and the sorting nexins Snx4/41/42 mediate distinct retrieval pathways from yeast endosomes. *EMBO J.* 22:548–557. https://doi.org/10.1093/emboj/cdg062

Hettema, E.H., J. Valdez-Taubas, and H.R.B. Pelham. 2004. Bsd2 binds the ubiquitin ligase Rsp5 and mediates the ubiquitination of transmembrane proteins. *EMBO J.* 23:1279–1288. https://doi.org/10.1038/sj.emboj.7600137

Huyghues-Despointes, B.M., J.M. Scholtz, and R.L. Baldwin. 1993. Helical peptides with three pairs of Asp-Arg and Glu-Arg residues in different orientations and spacings. *Protein Sci.* 2:80–85. https://doi.org/10.1002/pro.5560020108

Kamadurai, H.B., Y. Qiu, A. Deng, J.S. Harrison, C. Macdonald, M. Actis, P. Rodrigues, D.J. Miller, J. Souphron, S.M. Lewis, et al. 2013. Mechanism of ubiquitin ligation and lysine prioritization by a HECT E3. *eLife.* 2:e00828. https://doi.org/10.7554/eLife.00828

Kee, Y., N. Lyon, and J.M. Huibregtse. 2005. The Rsp5 ubiquitin ligase is coupled to and antagonized by the Ubp2 deubiquitinating enzyme. *EMBO J.* 24:2414–2424. https://doi.org/10.1038/sj.emboj.7600710

Kock, C., H. Arlt, C. Ungermann, and J.J. Heinisch. 2016. Yeast cell wall integrity sensors form specific plasma membrane microdomains important for signalling. *Cell. Microbiol.* 18:1251–1267. https://doi.org/10.1111/cmi.12635

Kota, J., M. Melin-Larsson, P.O. Ljungdahl, and H. Forsberg. 2007. Ssh4, Rcr2 and Rcr1 affect plasma membrane transporter activity in Saccharomyces cerevisiae. *Genetics.* 175:1681–1694. https://doi.org/10.1534/genetics.106.069716

Lauwers, E., Z. Erpapazoglou, R. Haguenauer-Tsapis, and B. André. 2010. The ubiquitin code of yeast permease trafficking. *Trends Cell Biol.* 20:196–204. https://doi.org/10.1016/j.tcb.2010.01.004

Léon, S., and R. Haguenauer-Tsapis. 2009. Ubiquitin ligase adaptors: regulators of ubiquitylation and endocytosis of plasma membrane proteins. *Exp. Cell Res.* 315:1574–1583. https://doi.org/10.1016/j.yexcr.2008.11.014

Léon, S., Z. Erpapazoglou, and R. Haguenauer-Tsapis. 2008. Ear1p and Ssh4p are new adaptors of the ubiquitin ligase Rsp5p for cargo ubiquitylation and sorting at multivesicular bodies. *Mol. Biol. Cell.* 19:2379–2388. https://doi.org/10.1091/mbc.e08-01-0068

Li, M., T. Koshi, and S.D. Emr. 2015a. Membrane-anchored ubiquitin ligase complex is required for the turnover of lysosomal membrane proteins. *J. Cell Biol.* 211:639–652. https://doi.org/10.1083/jcb.201505062

Li, M., Y. Rong, Y.-S. Chuang, D. Peng, and S.D. Emr. 2015b. Ubiquitin-dependent lysosomal membrane protein sorting and degradation. *Mol. Cell.* 57:467–478. https://doi.org/10.1016/j.molcel.2014.12.012

Li, Y., T. Kane, C. Tipper, P. Spatrick, and D.D. Jenness. 1999. Yeast mutants affecting possible quality control of plasma membrane proteins. *Mol. Cell. Biol.* 19:3588–3599. https://doi.org/10.1128/MCB.19.5.3588

Lin, C.H., J.A. MacGurn, T. Chu, C.J. Stefan, and S.D. Emr. 2008. Arrestin-related ubiquitin-ligase adaptors regulate endocytosis and protein turnover at the cell surface. *Cell.* 135:714–725. https://doi.org/10.1016/j.cell.2008.09.025

MacGurn, J.A., P.-C. Hsu, and S.D. Emr. 2012. Ubiquitin and membrane protein turnover: from cradle to grave. *Annu. Rev. Biochem.* 81:231–259. https://doi.org/10.1146/annurev-biochem-060210-093619

Mattiroli, F., and T.K. Sixma. 2014. Lysine-targeting specificity in ubiquitin and ubiquitin-like modification pathways. *Nat. Struct. Mol. Biol.* 21:308–316. https://doi.org/10.1038/nsmb.2792

Nakamura, N. 2011. The Role of the Transmembrane RING Finger Proteins in Cellular and Organelle Function. *Membranes (Basel).* 1:354–393. https://doi.org/10.3390/membranes1040354

O'Donnell, A.F. 2012. The running of the Buls: control of permease trafficking by α-arrestins Bul1 and Bul2. *Mol. Cell. Biol.* 32:4506–4509. https://doi.org/10.1128/MCB.01176-12

Perfetto, L., P.F. Gherardini, N.E. Davey, F. Diella, M. Helmer-Citterich, and G. Cesareni. 2013. Exploring the diversity of SPRY/B30.2-mediated interactions. *Trends Biochem. Sci.* 38:38–46. https://doi.org/10.1016/j.tibs.2012.10.001

Piao, H.L., I.M.P. Machado, and G.S. Payne. 2007. NPFXD-mediated endocytosis is required for polarity and function of a yeast cell wall stress sensor. *Mol. Biol. Cell.* 18:57–65. https://doi.org/10.1091/mbc.e06-08-0721

Piper, R.C., I. Dikic, and G.L. Lukacs. 2014. Ubiquitin-dependent sorting in endocytosis. *Cold Spring Harb. Perspect. Biol.* 6:a016808. https://doi.org/10.1101/cshperspect.a016808

Pizzirusso, M., and A. Chang. 2004. Ubiquitin-mediated targeting of a mutant plasma membrane ATPase, Pma1-7, to the endosomal/vacuolar system in yeast. *Mol. Biol. Cell.* 15:2401–2409. https://doi.org/10.1091/mbc.e03-10-0727

Radivojac, P., V. Vacic, C. Haynes, R.R. Cocklin, A. Mohan, J.W. Heyen, M.G. Goebl, and L.M. Iakoucheva. 2010. Identification, analysis, and prediction of protein ubiquitination sites. *Proteins.* 78:365–380. https://doi.org/10.1002/prot.22555

Ren, J., Y. Kee, J.M. Huibregtse, and R.C. Piper. 2007. Hse1, a component of the yeast Hrs-STAM ubiquitin-sorting complex, associates with ubiquitin peptidases and a ligase to control sorting efficiency into multivesicular bodies. *Mol. Biol. Cell.* 18:324–335. https://doi.org/10.1091/mbc.e06-06-0557

Rotin, D., O. Staub, and R. Haguenauer-Tsapis. 2000. Ubiquitination and endocytosis of plasma membrane proteins: role of Nedd4/Rsp5p family of ubiquitin-protein ligases. *J. Membr. Biol.* 176:1–17. https://doi.org/10.1007/s00232001079

Segarra, V.A., D.R. Boettner, and S.K. Lemmon. 2015. Atg27 tyrosine sorting motif is important for its trafficking and Atg9 localization. *Traffic.* 16:365–378. https://doi.org/10.1111/tra.12253

Shin, M.E., K.D. Ogburn, O.A. Varban, P.M. Gilbert, and C.G. Burd. 2001. FYVE domain targets Pib1p ubiquitin ligase to endosome and vacuolar membranes. *J. Biol. Chem.* 276:41388–41393. https://doi.org/10.1074/jbc.M105665200

Suzuki, S.W., and S.D. Emr. 2018. Membrane protein recycling from the vacuole/lysosome membrane. *J. Cell Biol.* 217:1623–1632. https://doi.org/10.1083/jcb.201709162

Tan, P.K., J.P. Howard, and G.S. Payne. 1996. The sequence NPFXD defines a new class of endocytosis signal in Saccharomyces cerevisiae. *J. Cell Biol.* 135:1789–1800. https://doi.org/10.1083/jcb.135.6.1789

Vowels, J.J., and G.S. Payne. 1998. A dileucine-like sorting signal directs transport into an AP-3-dependent, clathrin-independent pathway to the yeast vacuole. *EMBO J.* 17:2482–2493. https://doi.org/10.1093/emboj/17.9.2482

Wang, S., G. Thibault, and D.T. Ng. 2011. Routing misfolded proteins through the multivesicular body (MVB) pathway protects against proteotoxicity. *J. Biol. Chem.* 286:29376–29387. https://doi.org/10.1074/jbc.M111.233346

Wilk, S., J. Wittland, A. Thywissen, H.-P. Schmitz, and J.J. Heinisch. 2010. A block of endocytosis of the yeast cell wall integrity sensors Wsc1 and Wsc2 results in reduced fitness in vivo. *Mol. Genet. Genomics.* 284:217–229. https://doi.org/10.1007/s00438-010-0563-2

Zhang, Z.-R., J.S. Bonifacino, and R.S. Hegde. 2013. Deubiquitinases sharpen substrate discrimination during membrane protein degradation from the ER. *Cell.* 154:609–622. https://doi.org/10.1016/j.cell.2013.06.038

Zhao, Y., J.A. Macgurn, M. Liu, and S. Emr. 2013. The ART-Rsp5 ubiquitin ligase network comprises a plasma membrane quality control system that protects yeast cells from proteotoxic stress. *eLife.* 2:e00459. https://doi.org/10.7554/eLife.00459

Zhu, L., J.R. Jorgensen, M. Li, Y.-S. Chuang, and S.D. Emr. 2017. ESCRTs function directly on the lysosome membrane to downregulate ubiquitinated lysosomal membrane proteins. *eLife.* 6:e26403. https://doi.org/10.7554/eLife.26403